Measurement And Simulation Calculation of Wire Bow Angle During The Diamond Wire Saw Process

Zhiteng Xu
Huaqiao University
Hui Huang (huanghuihh@hotmail.com)
Huaqiao University
Changcai Cui
Huaqiao University

Research Article

Keywords: Wire saw, Wire bow angle, Simulation calculation

Posted Date: January 5th, 2022

DOI: https://doi.org/10.21203/rs.3.rs-1211134/v1

Version of Record: A version of this preprint was published at The International Journal of Advanced Manufacturing Technology on April 22nd, 2022. See the published version at https://doi.org/10.1007/s00170-022-09233-w.

Measurement and simulation calculation of wire bow angle during the diamond wire saw process

Zhiteng Xu[1] · Hui Huang[1] · Changcai Cui[1]

[1] Institute of Manufacturing Engineering, Huaqiao University, Xiamen 361021, China

Corresponding author:

Hui Huang

huanghuihh@hotmail.com

Abstract

The wire bow angle is an important factor that affects the shape precision of an ingot after the diamond wire sawing process. In this research, the wire bow angles of the inside and outside of an ingot were recorded with a high-speed camera. The effects of the processing parameters such as the wire tension force, feed speed, and wire speed on the wire bow angles inside and outside the ingot were analyzed. A numerical simulation model of the wire bow in the wire sawing process is presented in this paper to describe the wire bow angle inside the ingot. It was shown that the wire bow angle inside the ingot was smaller than that of outside the ingot for all of the processing parameters. The wire bow angles improved with the increase of the feed speed and decrease of the wire speed and the wire tension force. The results of the wire bow angle measurement of the inside ingot and the simulation calculation were similar for the process parameters.

Keywords Wire saw · Wire bow angle · Simulation calculation

1 Introduction

Diamond abrasive wire saw technology has been widely used to cut brittle and hard materials such as silicon, silicon carbide (SiC), and sapphire due to the higher efficiency, smaller kerf loss, and lack of size constraints [1]. During the cutting process, the contact force is found between the ingot and the diamond wire saw. Hence, the wire will bend to a certain extent and form a wire bow phenomenon, as shown in **Fig. 1.** The wire bow phenomenon during the wire sawing process will

reproduce itself on the surface of the ingot, causing saw marks with the same shape as the wire bow to emerge on the wafer surface. The wire will break and cause material waste when the wire bow angle is too large. Additionally, the ingots have shape accuracy deviation because the contact position between the ingot and the wire saw cannot reach the set coordinate point.

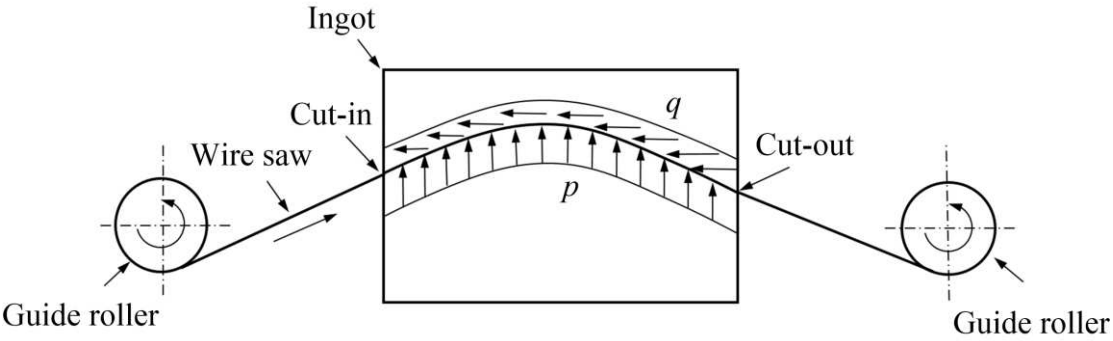

Fig. 1. Schematic of wire bow formation.

Clack et al. [2] used a non-contact capacitive sensor to measure the deviation distance of the wire saw of an outside ingot and calculate the wire bow angle. Liu et al. [3] used a high definition digital camera to take pictures of the wire bow angle outside an ingot. The stability of the wire bow angle during the cutting process was ensured by controlling the feed speed and the wire speed. Qin et al. [4] used the light projection method to measure the change in the wire saw projection position to control the wire bow angle. Wang et al. [5] applied the difference between the feed displacement and the saw slit depth to evaluate a diamond wire bow. In these detection methods, only the wire bow angle outside the ingot was measured.

Some scholars have established theoretical models of wire bow formation based on the principles of mechanics. Zhang et al. [6] divided a wire saw into a differential line for stress analysis during the cutting process, with the assumption that the wire saw was a continuum with some flexibility and elasticity in the process. Teomete [7] established a wire bow deflection model in which a uniform vertical load was applied in the middle of a wire saw. Liedke et al. [8] or Qiu et al. [9] derived the wire bow model for the wire sawing process description based on the macroscopic mechanical conditions.

Up to now, the accuracy of all the research models was verified by

experimentally obtaining the wire bow angle of the outside ingot. The difference in the force method of the wire saw inside and outside the ingot will inevitably lead to the deviation in the accuracy of the model. Therefore, a study towards the wire bow angle inside and outside the ingot will be analyzed to improve the accuracy of the wire bow model. A high-speed camera was used to measure the wire bow angle during a cutting experiment for transparent crystal. A numerical model of the wire bow deflection was established based on the force of the experimental results. The experimental results of the wire bow angle inside the ingot and the simulation calculation results were compared.

2 Wire sawing experiment

2.1. Experiment design

A single diamond wire sawing machine (JXQ-1201, No. 45, Research Institute of China Electronics Technology Group Corporation) was used for the wire sawing test in this research, as illustrated in **Fig. 2**. The distance L between the two guide rollers was 486 mm. A piezoelectric dynamometer was assembled on the workbench, and the experimental specimen was affixed to the dynamometer and located in the middle of the two guide rollers to guarantee the stability when the specimen was sawn. The wire tension force (T) of the wire could be adjusted by means of a pair of air cylinders. The wire saw ran with the wire speed (v_s) between two spools and reciprocated the direction periodically, and the reciprocating cycle time was 120 s, as shown in **Fig. 3.** The ingot was fed with a feed speed (v_f) in the vertical direction to achieve the material removal.

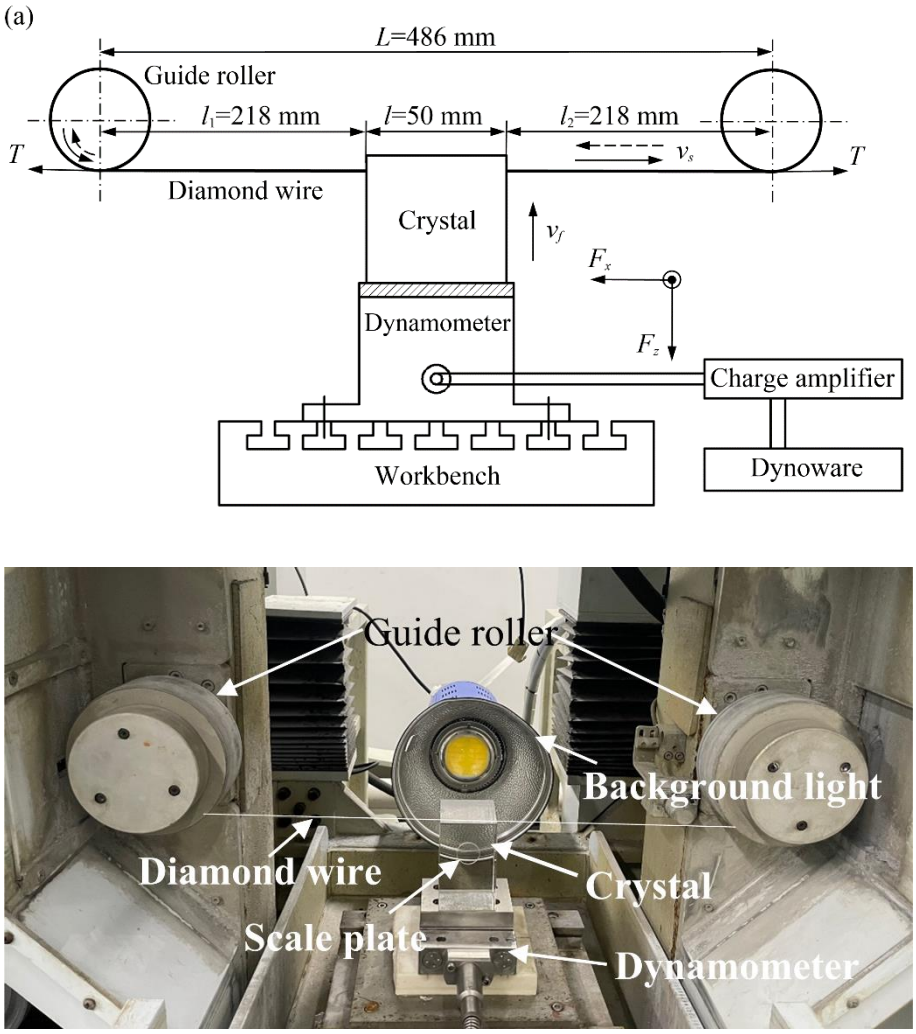

Fig. 2. Experimental design for a crystal sawn using a diamond wire saw.

(a) Schematic representation (b) Experiment system

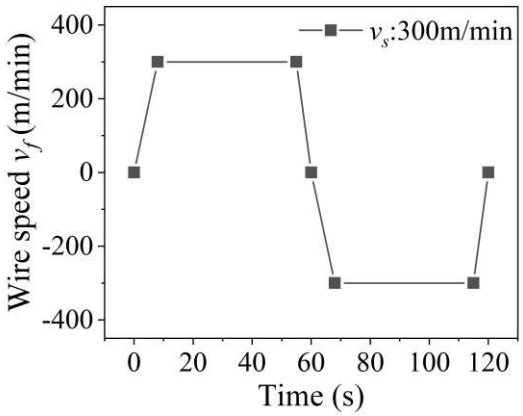

Fig. 3. Periodic reciprocating movement of the diamond wire saw.

A transparent K9 crystal was selected as the specimen material to make the wire bow angle inside the ingot measurable. The crystal was made up of 69.13% SiO_2,

10.75% B_2O_3, 10.4% Na_2O, and other oxides. The sawing length l of the crystal was 50 mm and the cutting depth was 30 mm in each experiment. The parameters of the wire sawing process are shown in **Table 1**.

Table 1 The wire sawing process parameters

Process parameters	Values
Wire tension force T (N)	15; 20; 25; 30; 35
Feeding speed v_f (mm/min)	0.2; 0.3; 0.4; 0.5; 0.6
Wire speed v_s (m/min)	200; 250; 300; 350; 400

Commercially available electroplated diamond wire was used for the sawing. A scanning electron microscopy (SEM) image of the surface topography of the wire was shown in **Fig. 4.** The diameter of the fixed diamond wire saw was 0.25 mm and the size of the diamond grit was 30–40 μm. The diamond wire saw had a length of approximately 10–16 grits/mm. To avoid the influence of wire wear on the experimental results, a new wire was adopted in each experiment.

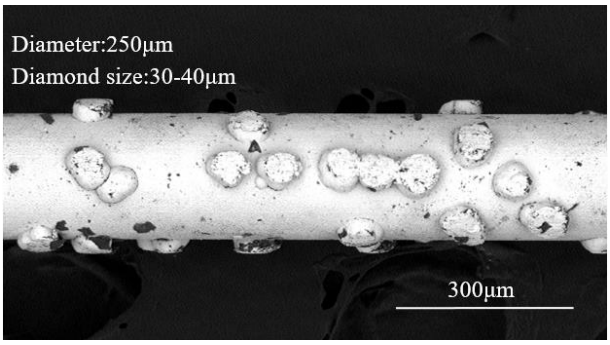

Fig. 4. SEM image of the fixed abrasive diamond wire saw.

2.2. Wire bow angle measurement

A high-speed camera (Phantom v2511) was used to take photographs of the sawing wire. The resolution of the camera was 1280 × 800 pixels, the sample rate was 1 kHz, and the exposure time was 9 μs. A high-brightness lamp was installed behind the sawing machine to improve the brightness and clarity of the photos taken, as shown in **Fig. 2(b)**. The original photograph was magnified ten times and the contrast was

adjusted. The intersection point between the sawing wire and the left side of the crystal in the photograph was set to the origin of the coordinates to establish the XOZ rectangular coordinate system, as shown in **Fig. 5**.

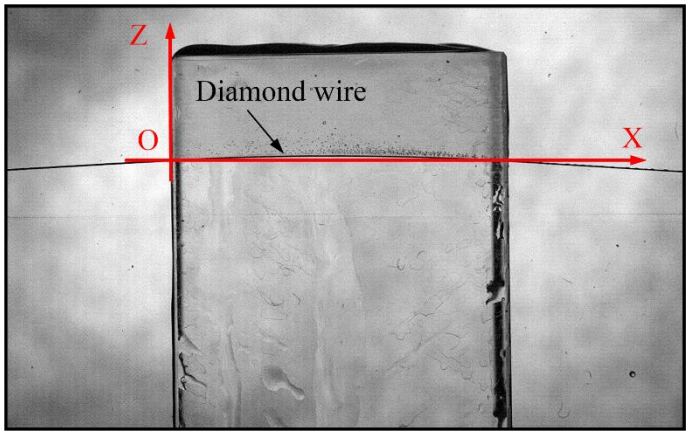

Fig. 5. Coordinate system establishment

2.3. Force measurement

The forces during sawing were recorded by a piezoelectric dynamometer (Kistler 9119AA2, Kistler Co., Ltd. Switzerland). The sampling frequency was 1 kHz. The force measurement experiment detected the force signals of the five reciprocating cycles before the completion of the wire saw cutting 30 mm depth. When the wire stopped moving, it was lifted manually to separate it from the specimen.

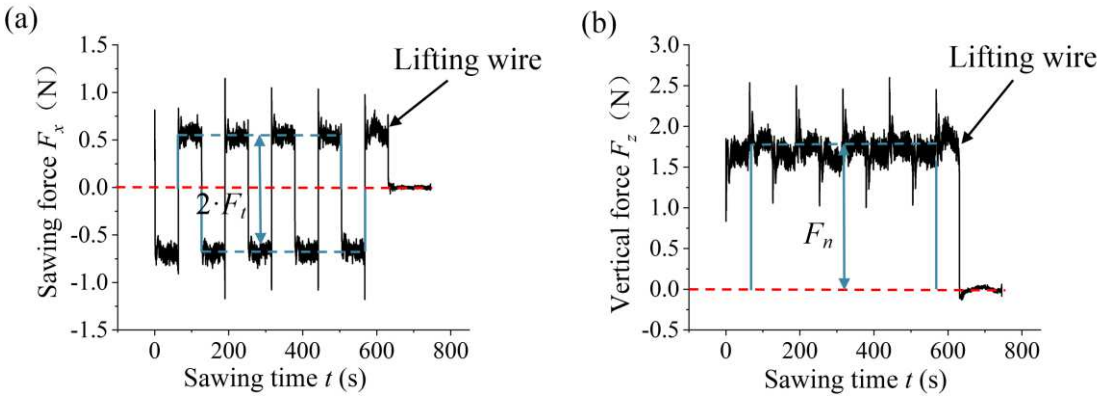

Fig. 6. Measurement of the force with the lifting of the wire.

(a) Horizontal direction (b) Vertical direction.

The force signals of the whole measurement process were deducted from the value of the baseline, and then a low-pass cutoff frequency of 3 Hz was applied to

determine the force value. The relationship between the sawing force and the sawing time is shown in **Fig. 6.** The tangential force (F_t) was obtained as half of the difference in the average value of the horizontal force (F_x) before and after a change in the sawing direction. The normal force (F_n) represents the average value of the vertical force (F_z).

3 Results

3.1 Simulation calculation model of the wire bow

The rectangular coordinate system was established with the highest point of the wire bow as the coordinate origin, as shown in **Fig. 7**. In the figure, l is the length of the ingot, and l_a is the horizontal distance between the highest point and the cut-in point. l_b is the horizontal distance between the highest point and the cut-out point.

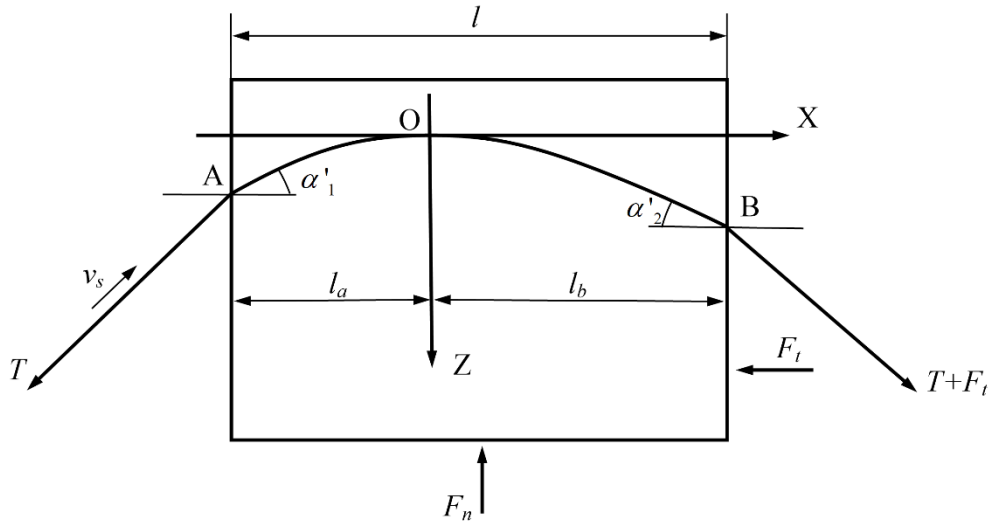

Fig. 7. Model of wire bow based on the macroscopic mechanism.

The wire deflection z of any point on the wire in the cutting zone could be derived as [10]:

$$z = \frac{F_{\mathrm{n}}}{2 \cdot H \cdot l + F_t \cdot x} x^2 \tag{1}$$

The horizontal tension H could be expressed as:

$$\left(H - \frac{F_t}{l} \cdot l_a \right)^2 + \left(\frac{F_n}{l} \cdot l_a \right)^2 = T^2 \tag{2}$$

The horizontal distance l_a and l_b could be expressed as:

$$\sqrt{(T+F_t)^2-\left[\frac{F_n}{l}\cdot(l-l_a)\right]^2}-\sqrt{T^2-(\frac{F_n}{l}\cdot l_a)^2}-F_t=0 \tag{3}$$

$$l_b=l-l_a \tag{4}$$

The slope of any point in the cutting zone could be expressed as:

$$z'=\frac{2\cdot F_n\cdot x}{2\cdot H\cdot l+F_t\cdot x}-\frac{F_n\cdot F_t\cdot x^2}{(2\cdot H\cdot l+F_t\cdot x)^2} \tag{5}$$

The wire bow angle of the inside of the ingot at the cut-in and cut-out position could be derived as:

$$\begin{cases}\alpha_1'=\arctan(z'_{|\,x=l_a})\\ \alpha_2'=\arctan(z'_{|\,x=l_b})\end{cases} \tag{6}$$

3.2 Experimental fitting model of the wire bow

The experimental fitting model of the wire bow was obtained by extracting and fitting the coordinate points of the photograph of the wire saw. The coordinates of 11 evenly divided discrete points on the left, inside, and right of the ingot in the picture were extracted respectively. The wire saw was affected by the normal force and the tangential force in the cutting zone, and the wire bow curve was approximately to a quadratic function according to **Eq. (2).** A quadratic polynomial was used to fit the discrete point coordinates on the wire saw of the inside ingot. The wire saw outside the ingot was tightened into a straight line with the wire tension force shown in **Fig. 7**, and the discrete point coordinates on the wire saw left and right of the ingot were therefore linearly fitted. Part of the length was taken to extract discrete points because the wire saw outside the ingot was linear.

The experimental fitting model of the wire bow is shown in **Fig. 8.** The fitting function of the wire saw was derived in order to obtain the slope, and then the wire bow angle was derived using the inverse trigonometric function. In the figure, α_1 and α_2 are the experimental value of the wire bow angle inside and outside ingot respectively in the cut-in position. θ_1 and θ_2 are the experimental value of the wire bow angle inside and outside ingot respectively in the cut-out position.

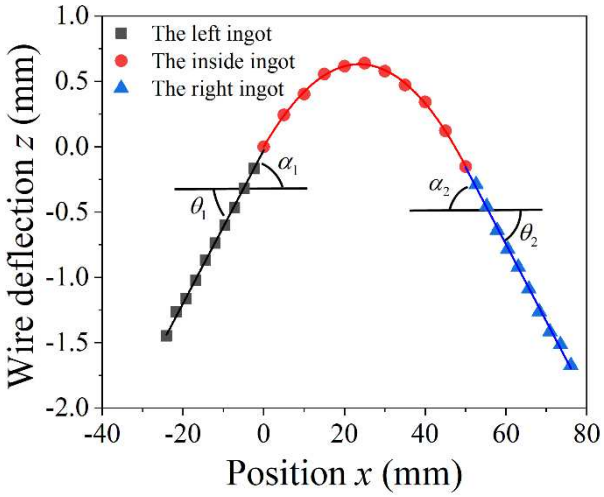

Fig. 8. Fit of the coordinate values of a discrete point on the sawing wire.

3.3 The effect of the wire saw reciprocating moves on the wire bow angle

The periodical reciprocate movement of the wire saw caused the cut-in position to change periodically on both sides of the ingot. The wire bow angle at the cut-in position was compared during the reciprocating motion, and a set of parameters was taken as an example, as shown in **Fig. 9.** The wire saw moved in a reciprocating direction has little influence on the wire bow angle for all of the processing parameters. Therefore, it is appropriate to analyze the experimental results of the positive direction movement of the wire saw.

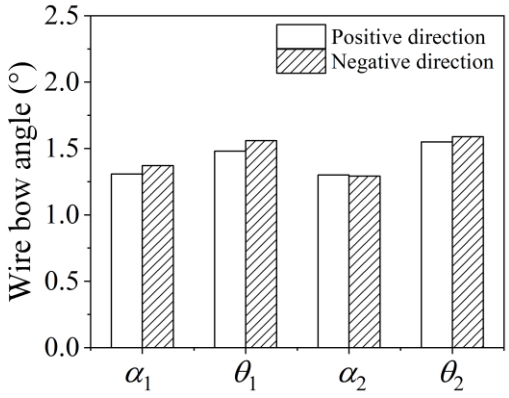

Fig. 9. The wire bow angle in reciprocating direction.

(Wire tension force: 25 N, Feed speed: 0.4 mm/min, Wire speed: 300 m/min)

3.4 The effect of the wire tension force on the wire bow angle

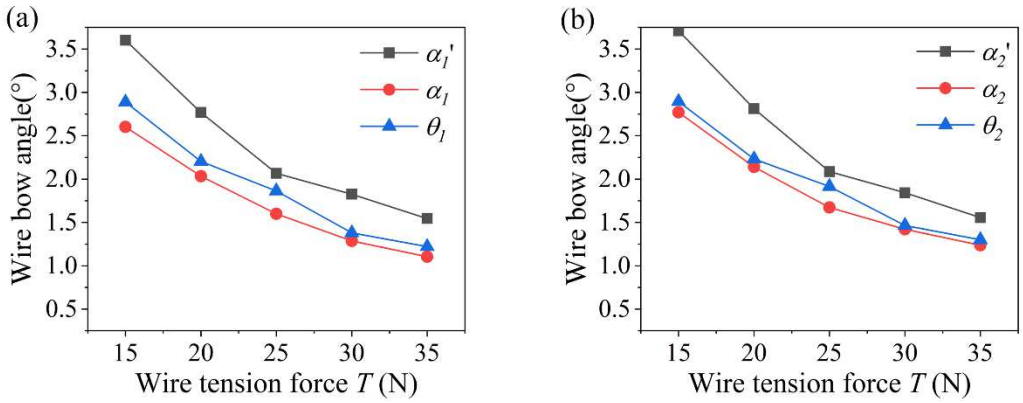

Fig. 10. The effect of the wire tension force on the wire bow angle.

(a) Cut-in position. (b) Cut-out position.

The effect of the wire tension force on the wire bow angle is shown in **Fig. 10.** In the figure, $\alpha_1^{'}$ and $\alpha_2^{'}$ are the simulation calculation value of the wire bow angle inside and outside the ingot respectively in the cut-in position. With an increase in the wire tension force from 15 N to 35 N, the simulation calculation value of the wire bow angle inside the ingot in the cut-in position decreased from 3.61° to 1.52°. The experimental values of the wire bow angle inside the ingot in the cut-in position decreased from 2.60° to 1.10°, and the wire bow angle outside the ingot in the cut-in position decreased from 2.89° to 1.22°.

Moreover, the tendency of the wire bow angle to change was gradually reduced with the increase of the wire tension force. The wire bow angles at the cut-in and cut-out positions were different with the increase of wire tension force, but the difference was only in the range of 0.05°. The wire bow angles at the cut-in and cut-out positions had the same variation.

3.5 The effect of the feed speed on the wire bow angle

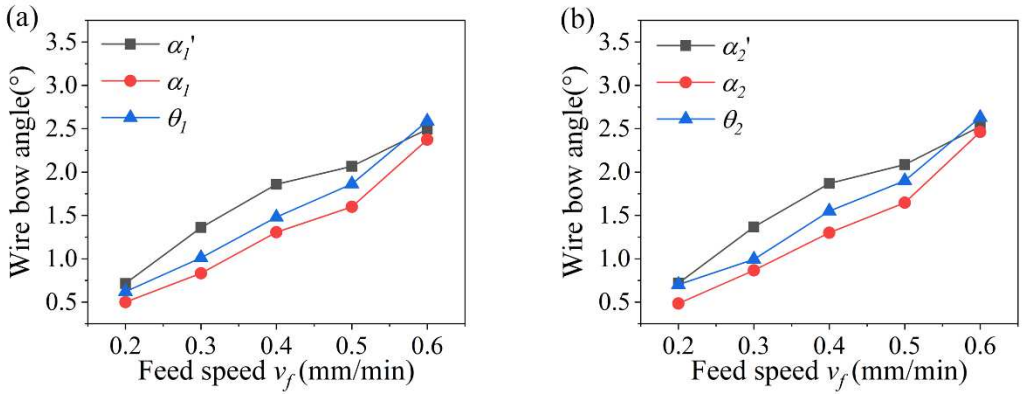

Fig.11. The effect of the feed speed on the wire bow angle.

(a) Cut-in position. (b) Cut-out position.

The effect of the feed speed on the wire bow angle is shown in **Fig. 11.** With an increase in the feed speeds from 0.2 mm/min to 0.6 mm/min, the simulation calculation value of the wire bow angle inside the ingot in the cut-in position increased from 0.71° to 2.46°. The experimental values of the wire bow angle inside the ingot in the cut-in position increased from 0.50° to 2.37°, and the wire bow angle outside the ingot in the cut-in position decreased from 0.62° to 2.59°. The wire bow angle improved linearly with the increase of the feed speed.

3.6 The effect of the wire speed on the wire bow angle

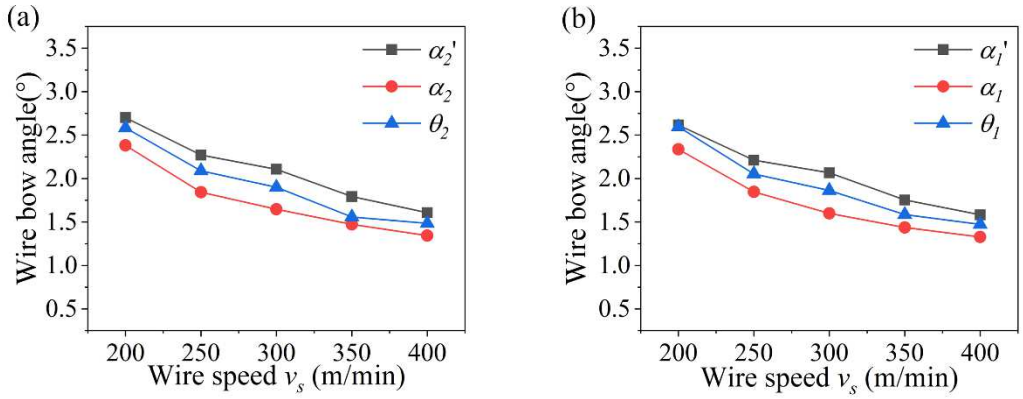

Fig. 12. The effect of the wire speed on the wire bow angle.

(a) Cut-in position. (b) Cut-out position.

The effect of the wire speed on the wire bow angle is shown in **Fig. 12.** With an increase in the wire speed from 200 m/min to 400 m/min, the simulation calculation value of the wire bow angle inside the ingot in the cut-in position decreased from 2.57° to 1.57°. The experimental values of the wire bow angle inside the ingot in the cut-in position decreased from 2.34° to 1.33°, and the wire bow angle outside the ingot in the cut-in position decreased from 2.60° to 1.47°. The tendency of the wire bow angle to change was gradually reduced with the wire speed increase.

In brief, the wire bow angles of the outside ingot were all larger than those of the inside for the wire tension forces in the range of 15 N to 35 N, the feed speeds in the range of 0.2 mm/min to 0.6 mm/min, and the wire speeds in the range of 200 m/min to 400 m/min. The wire tension force and the feed speed had the greatest influence on the wire bow angle and the wire speed had the least influence on the wire bow angle.

The variation trends of the wire bow angle for the experiment and the simulation calculation results were similar. The wire bow angles improved with the increase of the feed speed and decrease of the wire speed and the wire tension force. The simulation calculation values were slightly larger than the experimental values because the wire saw was assumed to be an ideal string and the force load was a uniform load.

4 Discussion

According to the simulation calculation model of the wire bow in **Fig. 7**, the factors that affect the wire bow angle include wire tension force, tangential force and normal force. Wang et al. [11] found that the sawing force increases approximately linearly with feed speed, and decreases nonlinearly with wire speed during the sawing process. The reason is related to the volume of material removal per length of wire (q). According to the wire saw kinematics in the sawing process, the volume of material removal per length of wire (q) could be expressed as:

$$q = \frac{bwv_f}{v_s} \tag{7}$$

Where b is the slit width and w is the cutting length of the specimen. Here, the

slit width b can be approximate equal to the diameter of the fixed diamond wire saw 0.25 mm, and the cutting length w is equal to sawing length l =50 mm. When the width of the saw slit width and the cutting length of the specimen were constant, the removal volume per length of the wire saw had a linear relationship with the feed speed and an inverse proportional function relationship with the wire speed. The effect of the volume of material removal per length on the wire bow angle of the inside ingot in cut-in position is shown in **Fig. 13.**

The wire bow angles are found to be approximately proportional to the volume of material removal per length of wire, and the wire bow angle approximately reflected the volume of material removal per length of the wire. During the wire saw cutting process, the wire bow angles of the outside ingot were larger than those of the inside ingot for processing parameters to ensure the cutting ability of the wire saw.

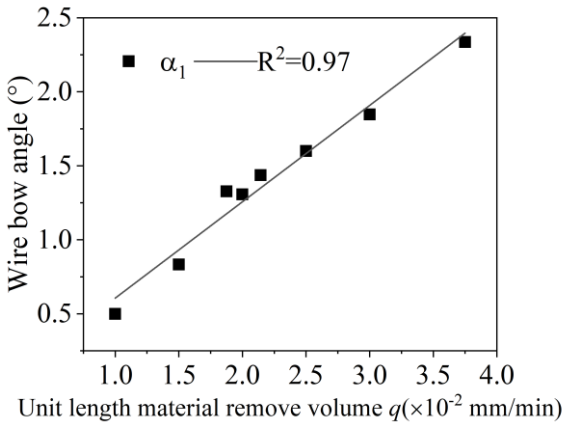

Fig. 13. Effect of the unit length material removal volume on the wire bow angle

5 Conclusion

(1) The wire bow angle of the outside was larger than that of the inside in order to ensure the cutting ability of the wire saw during the whole wire saw cutting process.

(2) The simulation calculation and experimental results showed that the wire bow angles improved with the increase of the feed speed, the decrease of the wire speed, and the wire tension force

(3) The experimental results showed that the wire bow angle is approximately proportional to the volume of material removal per length of wire, and the wire bow angle approximately reflected the volume of material removal per length of wire.

Acknowledgements

Zhiteng Xu, Hui Huang would like to acknowledge the financial supports from the National Natural Science Foundation of China (51375179, U1805251), from the Changjiang Scholars and Innovative Research Team in University (IRT_17R41), and from the Major Science and Technology Project of Xiamen City (3502ZCQ20191007).

References

1. Wu H (2016) Wire sawing technology: A state-of-the-art review. Precis Eng 43:1–9. https://doi.org/10.1016/j.precisioneng.2015.08.008
2. Clark WI, Shih AJ, Hardin CW, et al (2003) Fixed abrasive diamond wire machining - Part I: Process monitoring and wire tension force. Int J Mach Tools Manuf 43:523–532. https://doi.org/10.1016/S0890-6955(02)00215-8
3. Liu T, Ge P, Bi W, Gao Y (2020) A new method of determining the slicing parameters for fixed diamond wire saw. Mater Sci Semicond Process 120:105252. https://doi.org/10.1016/j.mssp.2020.105252
4. Qin W, Zhidong L, Lida S, et al (2017) Test research on wire deflection detection of a diamond wire saw. Int J Adv Manuf Technol 91:1347–1354. https://doi.org/10.1007/s00170-016-9787-6
5. Wang J, Jia Z, Guo YB (2018) Shape-cutting of quartz glass by spark discharge-assisted

diamond wire sawing. J Manuf Process 34:131–139. https://doi.org/10.1016/j.jmapro.2018.06.001

6. ZHANG Liaoyuan，WANG Chao，WANG Jianguang YY (2012) Research on Cutting Trajectory of Electroplated Diamond Wire Saw. J China Ordnance 8:6–10
7. Teomete E (2008) Mechanics of wire saw machining process: Experimental analyses and modeling. Iowa State Univ Diss Theses - Gradworks. https://doi.org/10.13537/j.issn.1004-3918.2008.09.007
8. Liedke T, Kuna M (2011) A macroscopic mechanical model of the wire sawing process. Int J Mach Tools Manuf 51:711–720. https://doi.org/10.1016/j.ijmachtools.2011.05.005
9. Qiu J, Li X, Ge R, et al (2020) Formation mechanism of wire bow and its influence on diamond wire saw process and wire cutting capability. Int J Mech Sci 185:. https://doi.org/10.1016/j.ijmecsci.2020.105851
10. Li BZ (2008) Echnical manual for construction of high voltage overhead transmission line. China Electric Power Press.
11. Wang P, Ge P, Gao Y, Bi W (2017) Prediction of sawing force for single-crystal silicon carbide with fixed abrasive diamond wire saw. Mater Sci Semicond Process 63:25–32. https://doi.org/10.1016/j.mssp.2017.01.014

Statements & Declarations

The authors declared that they have no conflicts of interest to this work.

We declare that we do not have any commercial or associative interest that represents a conflict of interest in connection with the work.

Funding

This work was supported by the National Natural Science Foundation of China (51375179, U1805251), the Changjiang Scholars and Innovative Research Team in University (IRT_17R41), and the Major Science and Technology Project of Xiamen City (3502ZCQ20191007).

Competing Interests

The authors have no relevant financial or non-financial interests to disclose.

Author Contributions

All authors contributed to the study conception and design. Zhiteng Xu is the executor of article writing and experiment operation. Hui Huang contributed to the conception of the work. Changcai Cui reviewed and edited the paper. All authors read and approved the final manuscript.